Synchrotron-radiation x-ray multiple diffraction applied to the study of electric-field-induced strain in an organic nonlinear optical material

L. H. Avanci* and L. P. Cardoso
Instituto de Física ''Gleb Wataghin,'' UNICAMP, Caixa Postal 6165, CEP 13083-970, Campinas, SP, Brazil and Pure and Applied Chemistry Department, University of Strathclyde, Glasgow G1 1XL, United Kingdom

J. M. Sasaki,† S. E. Girdwood,‡ and K. J. Roberts
Centre for Molecular and Interface Engineering, Department of Mechanical and Chemical Engineering, Heriot-Watt University, Riccarton, Edinburgh EH14 4AS, United Kingdom

D. Pugh and J. N. Sherwood
Pure and Applied Chemistry Department, University of Strathclyde, Glasgow G1 1XL, United Kingdom
(Received 24 September 1999)

In this work, distortions produced in the unit cell of a MBANP [(−)-2-(α-methylbenzylamino)-5-nitropyridine] nonlinear organic crystal under the influence of an applied electric field, $\vec{E}$, are investigated by using synchrotron-radiation x-ray multiple diffraction (XRMD). The method is based in the inherent sensitivity of this technique to determine small changes in the crystal lattice, which provide peak position changes in the XRMD pattern (Renninger scan). A typical Renninger scan shows numerous secondary peaks, each one carrying information on one particular direction within the crystal. The (hkl) peak position in the pattern, for a fixed wavelength, is basically a function of the unit cell lattice parameters. Thus small changes in any parameter due to a strain produced by $\vec{E}$ give rise to a corresponding variation in the (hkl) peak position and the observed strain is related to the piezoelectric coefficients. The advantage of this method is the possibility of determining more than one piezoelectric coefficient from a single Renninger scan measurement [L. H. Avanci, L. P. Cardoso, S. E. Girdwood, D. Pugh, J. N. Sherwood, and K. J. Roberts, Phys. Rev. Lett. **81**, 5426 (1998)]. The method has been applied to the MBANP (monoclinic, point group 2) crystal and we were able to determine four piezoelectric coefficients: $|d_{21}|=0.2(1)\times10^{-11}\,\mathrm{CN}^{-1}$, $|d_{22}|=24.8(3)\times10^{-11}\,\mathrm{CN}^{-1}$, $|d_{23}|=1.3(1)\times10^{-11}\,\mathrm{CN}^{-1}$, and $|d_{25}|=5.9(1)\times10^{-11}\,\mathrm{CN}^{-1}$. The measurements were carried out using the SRS stations 16.3, Daresbury Laboratory, Warrington, UK.

I. INTRODUCTION

The investigation of nonlinear optical effects in organic crystals has been a very active area of research over the past decade.[1–7] The primary motivation for this activity has been the realization that some organic molecules have exceptionally large second order polarizabilities (first hyperpolarizabilities) compared with many inorganic materials. The possibilities of exploiting this fundamental property are perceived to be extensive because of the almost endless variation in chemical structure that can be produced through modern organic synthesis. The nonlinear responses of crystals have their origins in the (fairly predictable) molecular nonlinearities,[8] but the crystal structure and intermolecular interactions in the crystal also play a crucial part in determining the nature of the effects produced. For a second order response, the crystal must be noncentrosymmetric and the most effective space groups are often those which also show piezoelectricity. For an effective transverse linear electro-optic effect (LEO) the usual model requires that the polar axes of the constituent molecules should be as well aligned as possible, while for phase-matched second harmonic generation (SHG) a certain optimum angle between the polar axes of non-equivalent molecules is expected to be most efficient. The LEO effect as a function of optical frequency[9] in MBANP has been studied as well as SHG.[10–13] SHG is a purely high frequency phenomenon involving only fields at optical frequencies, whilst the LEO effect is produced by the interaction of an optical field with a low frequency field via the second-order susceptibility. The inverse piezoelectric effect and the stress-strain response embodied in the elastic constants involve only low frequencies.

High-resolution x-ray diffraction techniques provide optimum tools for studying the minute motion of lattice planes associated with the application of electric fields to nonlinear optical crystals. Using techniques such as x-ray multiple diffraction (XRMD),[14] we can assess changes in the lattice parameters and crystal symmetry as a function of field strength. Such approaches, when coupled with the use of synchrotron radiation enable, in principle, diffraction measurements to be carried out dynamically. Thus the effects associated with lattice relaxation at low frequencies can be isolated from the remaining high frequency electronic process, which are in principle calculable from the SHG susceptibilities. The interpretation of the whole range of nonlinear optic effects will therefore, to some extent, be clarified by unambiguous identification of the low frequency contributions.

The first objective of our study was to apply the XRMD technique to investigate the distortion of the crystal lattice under the influence of an external electric field and to assess

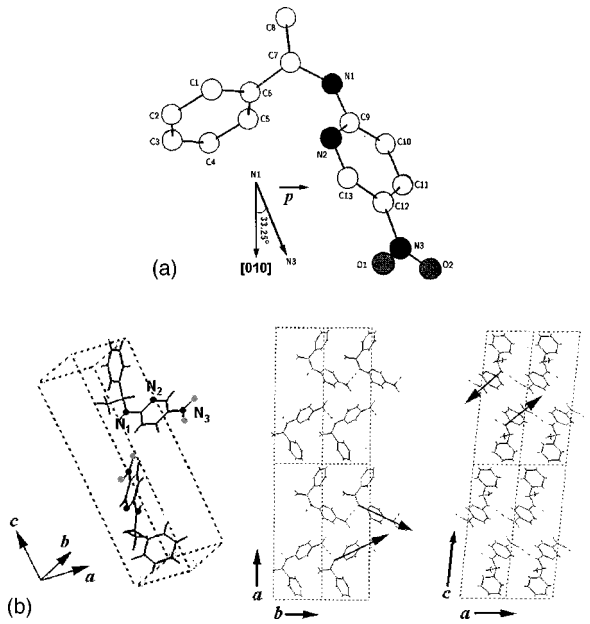

FIG. 1. (a) The MBANP molecule. The molecular dipole moment $\vec{p}$ is indicated. (b) Projections of the MBANP in two different planes showing the polar nature of the $\vec{b}$ axis.

the feasibility of determining the piezoelectric coefficient by this method. We describe calculations derived to relate electric field strength, E, strain, ϵ_{ij}, changes in the lattice parameters $(\Delta a, \Delta b, \Delta c, \Delta\beta)$, and changes in the peak positions in an x-ray pattern $(\Delta\omega^{00l}, \Delta\phi^{hkl})$ from which the piezoelectric coefficients will be determined.

II. BACKGROUND

A. MBANP

MBANP (Ref. 15) [(−)-2-(α-methylbenzylamino)-5-nitropyridine] molecular formula $C_{13}H_{13}N_3O_2$, crystallizes in the monoclinic space group $P2_1$, point group 2 with unit cell [Fig. 1(b)] dimensions of $a=5.392$ Å, $b=6.354$ Å, $c=17.924$ Å, and $\beta=94.60°$. The MBANP molecule [Fig. 1(a)] is butterfly shaped containing two aromatic rings angled at 84.6°. Charge transfer occurs between the amino nitrogen (donor) and nitro nitroge nitrogen (acceptor) so that the molecular dipole moment $\vec{p}$ has its largest component in the (001) direction at an angle of 33.25° to the unique axis $\vec{b}$. The crystallographic data of the MBANP are given in Table 1.[15]

Intermolecular hydrogen bonding occurs in the [011] direction between molecules related by a [1,1,0] translation. Due to this, MBANP can contribute to wave propagation in both [010] and [001] directions. Although hydrogen bonding does not have a great effect on the molecular shape it does play an important role in imposing a strong net alignment of the molecular dipoles within the material [Fig. 1(b)]. The alignment of the molecular dipoles contributes to the optical nonlinearity of the material. In MBANP the chiral methylbenzylamino group causes noncentrosymmetry and the nitro (acceptor) and amino (donor) provide the polarizable functionality, which are needed for second harmonic generation. Hyperpolarizability in MBANP is due chiefly to the dipole moment of the pyridine fragment.

B. Lattice distortions, strain, and piezoelectric effects in monoclinic crystals

The relationship between changes in the unit cell parameters, which can, in principle, be determined by XRMD, and the piezoelectric coefficients are given by standard tensor transformations. Since, as far as we can ascertain, they have not been used in this context in the literature, we give here a brief derivation of the formulas. The first part of this derivation is general, but the final formulas are specialized for the case under consideration in this paper, a monoclinic crystal of point group 2. The tensor summation convention over repeated indices is implied whenever one or more suffixes, i, j, or k is repeated in an expression.

First, changes in any vector, $\vec{r}=\{r_i\}$ and the angle, θ, between any two vectors, $\vec{r}$ and $\vec{s}$, are written in terms of the strain tensor, ε_{ij}. From the definition of strain tensor, $\Delta r_i = \varepsilon_{ij} r_j$. Differentiating the equations for the squared length of a vector and the cosine of the angle,

$$r^2 = r_i r_j, \quad \cos\theta = \frac{r_i s_i}{rs},$$

leads to

$$\Delta r = \frac{r_i r_j}{r}\varepsilon_{ij},$$

$$\Delta\theta = \frac{1}{\sin\theta}\left[-\frac{r_i s_j + s_i r_j}{rs} + \cos\theta\left\{\frac{r^2 s_i s_j + s^2 r_i r_j}{(rs)^2}\right\}\right]\varepsilon_{ij} \tag{1}$$

TABLE I. Crystallographic data of MBANP.

MBANP ($C_{13}H_{13}N_3O_2$): (−)-2-(α-methylbenzylamino)-5-nitropyridine	Structure factors @ (23±1)°
Crystal class: Monoclinic	$F(1\bar{1}3)=796(100\%)$
$a=5.409(3)$ Å, $b=6.371(1)$ Å,	$F(00\bar{6})=74$
$c=17.968(6)$ Å, $\beta=94.6°$	
Space group: $P2_1$	$F(200)=110$
Point group: 2	$F(020)=352$
Polar axis: $\vec{b}\equiv[010]$	$F(101)=720$
Molecules per unit cell:2	

for the changes in r and θ. These equations are used to calculate the changes in the lattice constants, a, b, c, α, β and γ. The piezoelectric tensor is defined in terms of the strain induced by a field, $\vec{E}$, as

$$\varepsilon_{ij} = d_{ijk} E_k . \tag{2}$$

For a monoclinic crystal of point group 2, using matrix (Voigt) notation we have

$$\begin{pmatrix} \varepsilon_{xx} \\ \varepsilon_{yy} \\ \varepsilon_{zz} \\ 2\varepsilon_{yz} \\ 2\varepsilon_{zx} \\ 2\varepsilon_{xy} \end{pmatrix} = \begin{pmatrix} 0 & d_{21} & 0 \\ 0 & d_{22} & 0 \\ 0 & d_{23} & 0 \\ d_{14} & 0 & d_{34} \\ 0 & d_{25} & 0 \\ d_{16} & 0 & d_{36} \end{pmatrix} \begin{pmatrix} E_x \\ E_y \\ E_z \end{pmatrix}, \tag{3}$$

where the positions of zeros are determined by crystal symmetry. For a monoclinic crystal, the pattern of nonzero matrix elements remains the same provided the y axis is identified as the monoclinic axis, $\vec{b}$, and $\vec{x}$, $\vec{y}$, $\vec{z}$ form an orthogonal triad. The conventional choice of the standard piezoelectric system ($\vec{x} \rightarrow \vec{a}^*$, $\vec{y} \rightarrow \vec{b}$, $\vec{z} \rightarrow \vec{c}$) is used here. Note the transposed row and column suffixes in the standard d matrix.[16]

1. Case (a): Field aligned with $\vec{b}$; $\vec{E} = (0, E_y, 0)$

The only nonzero strain components are then

$$\varepsilon_{xx} = d_{21} E_y ,$$

$$\varepsilon_{yy} = d_{22} E_y ,$$

$$\varepsilon_{zz} = d_{23} E_y ,$$

$$\varepsilon_{zx} = (1/2) d_{25} E_y . \tag{4}$$

Therefore using Eqs. (2) and (3) we obtain

$$\frac{1}{E_y}\frac{\Delta a}{a} = d_{21}\sin^2\beta + d_{23}\cos^2\beta + \frac{1}{2} d_{25}\sin(2\beta), \tag{5}$$

$$\frac{1}{E_y}\frac{\Delta b}{b} = d_{22}, \tag{6}$$

$$\frac{1}{E_y}\frac{\Delta c}{c} = d_{23}, \tag{7}$$

and

$$\frac{1}{E_y}\Delta\beta = \frac{1}{2}\sin(2\beta)(d_{21} - d_{23}) - \sin^2(\beta) d_{25}. \tag{8}$$

The angles α and γ do not change from 90°. The principal diagonal component, d_{22} is determined directly from the change in b and d_{23} from the change in c. The two remaining simultaneous equations can be solved to find d_{21} and d_{25}.

2. Case (b): Field orthogonal to $\vec{b}$; $\vec{E} = (E_x, 0, E_z)$

The nonzero strain components are

$$\varepsilon_{yz} = \frac{1}{2}(d_{14} E_x + d_{34} E_z), \quad \varepsilon_{xy} = \frac{1}{2}(d_{16} E_x + d_{36} E_z). \tag{9}$$

It follows from Eq. (1) that, in this case, $\Delta a = \Delta b = \Delta c = \Delta\beta = 0$, but the angles α and γ are changed from 90°, so that the lattice is distorted into a triclinic structure. From Eqs. (1) and (3),

$$-\frac{1}{2}\Delta\alpha = \varepsilon_{yz}, \quad -\frac{1}{2}\Delta\gamma = \cos\beta\,\varepsilon_{yz} + \sin\beta\,\varepsilon_{xy}. \tag{10}$$

[The lack of symmetry in these equations is a consequence of the arbitrary choice of the piezoelectric system of axes]. Using Eqs. (6) and (7) gives, finally,

$$-\Delta\alpha = d_{14} E_x + d_{34} E_z ,$$

$$-\Delta\gamma = (\cos\beta\, d_{14} + \sin\beta\, d_{16}) E_x + (\cos\beta\, d_{34} + \sin\beta\, d_{36}) E_z . \tag{11}$$

If, for example, the field is applied along the $\vec{a}^*$ axis, $\vec{E} = (E_x, 0, 0)$, then d_{14} and d_{16} can be found. A second experiment, with the field along $\vec{c}$, will allow the two remaining coefficients to be extracted.

C. X-ray multiple diffraction

X-ray multiple diffraction is a technique which has been used by several authors[17–21] to provide a physical solution to the important crystallographic phase problem. In this work, the multiple beam effects depend only on the geometry in reciprocal space, not on the phase sensitive interference. The multiple diffraction phenomenon arises when an incident beam simultaneously satisfies the Bragg law for more than one set of planes within a crystal. The primary diffracted beam is produced by a set of planes, called primary planes (h_p, k_p, l_p). By rotating the sample around the primary reciprocal lattice vector, several secondary planes (h_s, k_s, l_s) within the crystal with arbitrary orientation also diffract. The intensity interactions among the primary and the several secondary reflections are established through the coupling reflection $(h_p\text{-}h_s, k_p\text{-}k_s, l_p\text{-}l_s)$. In the Renninger scanning (RS) method,[22] the crystal is aligned for Bragg (single or two beam) diffraction and the sample rotate around the Bragg plane normal to produce a diffraction pattern with a series of multiply diffracted (n beam where $n > 2$) beams superimposed on a Bragg diffracted ''background.'' When the relative strengths of the reflections involved in a multiple beam process interfere constructively we get an enhancement of intensity (Umweganregung), whereas in the converse case we get a reduction of intensity (Aufhellung). The number of symmetry mirrors appearing in a RS are determined by the primary vector symmetry and the reciprocal lattice points rotation about that vector, when they enter and leave the Ewald sphere. The technique have recently been applied to the study of lattice coherence in heteroepitaxial systems.[23,24]

The inherent sensitivity to microcrystallographic changes of Renninger scanning x-ray multiple diffraction makes this technique an ideal candidate for examining the subtle

changes in the lattice geometry of nonlinear optic materials when subjected to an external stimulus. Thus one can collect XRMD data as a function of electric field and use data to deduce the piezoelectric tensors. Additionally, the dynamics of lattice changes can also be determined using the time resolution capability offered by the use of a high synchrotron radiation source. Using this approach fundamental data important for the molecular and crystal engineering of novel nonlinear optic device materials can, in principle, be produced.

The angular positions of any secondary (hkl) multiple diffraction peaks in a RS can be measured in terms of an angle, $\beta = \phi^{hkl} \pm \phi_0$ (the signal stands for the entrance and exit of the secondary reciprocal lattice point on the Ewald sphere), where ϕ_0 is the angle between the secondary vector and the primary incidence plane measured on the ES equatorial plane.[25] This angle is given by

$$\cos(\phi^{hkl} \pm \phi_0) = \frac{1}{2} \frac{(H^2 - \vec{H}\cdot\vec{H}_0)}{\sqrt{1/\lambda^2 - H_0^2/4}\sqrt{H^2 - H_p^2}}, \tag{12}$$

where λ is the wavelength of the incident beam and $\vec{H}_0$ is the primary vector, $\vec{H}$ is the secondary vector and, $\vec{H}_p = (\vec{H}\cdot\vec{H}_0)(\vec{H}_0/H_0^2)$. These vectors, for a monoclinic crystal, are functions of the unit cell lattice parameters a, b, c and β, so that we can write

$$\cos(\phi^{hkl} \pm \phi_0) \equiv f(a,b,c,\beta). \tag{13}$$

For the MBANP case with the field applied along the monoclinic [010] axis and the primary reflection being $(00l_0)$ with $l_0 = -6$, Eq. (9) has the form

$$\cos(\phi^{hkl} \pm \phi_0)$$

$$= \frac{1}{2} \frac{\dfrac{h^2}{a^2 \sin^2\beta} + \dfrac{k^2}{b^2} + \dfrac{l(l-l_0)}{c^2 \sin^2\beta} - \dfrac{hl_0 \cos\beta}{ac \sin^2\beta}}{\sqrt{\dfrac{1}{\lambda^2} - \dfrac{l_0^2}{4c^2 \sin^2\beta}}\sqrt{\dfrac{h^2}{a^2} + \dfrac{k^2}{b^2} - \dfrac{2hl\cos\beta}{ac \sin^2\beta}}}$$

$$= f(a,b,c,\beta). \tag{14}$$

In order to obtain the variation in the four unit cell parameters that characterize this system the differential coefficients appearing in the equation should be determined as

$$-\sin(\phi^{hkl} \pm \phi_0)\Delta(\phi^{hkl} \pm \phi_0) = \left.\frac{\partial f}{\partial a}\right|_{hkl} \Delta a + \left.\frac{\partial f}{\partial b}\right|_{hkl} \Delta b + \left.\frac{\partial f}{\partial c}\right|_{hkl} \Delta c + \left.\frac{\partial f}{\partial \beta}\right|_{hkl} \Delta\beta. \tag{15}$$

Thus, for each analyzed *hkl* secondary reflection the variation in the unit cell are given by the following.

1. Secondary reflection h00

$$\frac{\Delta a}{a}\left(\left.\frac{\partial f}{\partial a}\right|_{h00}\right) = \tan(\phi^{h00} \pm \phi_0)\Delta(\phi^{h00} \pm \phi_0) + \frac{\Delta c}{c}\left(\left.\frac{\partial f}{\partial c}\right|_{h00}\right) + \Delta\beta\left(\left.\frac{\partial f}{\partial \beta}\right|_{h00}\right). \tag{16}$$

2. Secondary reflection 0k0

$$\frac{\Delta b}{b}\left(\left.\frac{\partial f}{\partial b}\right|_{0k0}\right) = \tan(\phi^{0k0} \pm \phi_0)\Delta(\phi^{0k0} \pm \phi_0) + \frac{\Delta a}{a}\left(\left.\frac{\partial f}{\partial a}\right|_{0k0}\right) + \Delta\beta\left(\left.\frac{\partial f}{\partial c}\right|_{0k0}\right). \tag{17}$$

3. Secondary reflection h0l

Finally, the last equation obtained from the x-ray multiple diffraction is

$$\Delta\beta\left(\left.\frac{\partial f}{\partial \beta}\right|_{h0l}\right) = \tan(\phi^{h0l} \pm \phi_0)\Delta(\phi^{h0l} \pm \phi_0) + \Delta a\left(\left.\frac{\partial f}{\partial a}\right|_{h0l}\right) + \Delta c\left(\left.\frac{\partial f}{\partial c}\right|_{h0l}\right). \tag{18}$$

4. Primary reflection 00l_0

The fourth necessary equation to determine the piezoelectric coefficients can be directly derived from Bragg law, $\lambda = 2d\sin(\omega_{\text{Bragg}}^{00l_0})$. When

$$\frac{1}{d_{00l_0}} = \frac{l_0}{c\sin\beta}, \tag{19}$$

one finds

$$\frac{\Delta c}{c} = -\cot(\omega_{\text{Bragg}}^{00l_0})\Delta(\omega_{\text{Bragg}}^{00l_0}) - \cot\beta\Delta\beta. \tag{20}$$

Equations (16), (17), (18), and (20) form a set of coupled equations with variables: $\Delta a/a, \Delta b/b, \Delta c/c$, and $\Delta\beta$. This system, in principle, is solvable and then it allows for the determination of the distortions produced by E_y in the crystalline unit cell. The distortions are determined from the $h00$, $0k0$ and $h0l$ peak position variation in the Renninger scan and, from the $00l_0$ peak change in the rocking curve. As discussed before, the distortions are related to the piezoelectric coefficients d_{21}, d_{22}, d_{25}, and d_{23}, through early derived equations (5)–(8).

5. Strain as a function of changes in the x-ray diffraction peak positions

In the determination of the piezoelectric coefficients, the secondary reflections $h00 = 200$, $0k0 = 020$ and $h0l = 101$ and, the primary reflection $00l_0 = 00\bar{6}$ have been chosen. By using the lattice constants from Table I and the wavelength $\lambda = 1.4878$ Å, the system of equations was solved giving the variations in lattice parameters. We have used the parameter

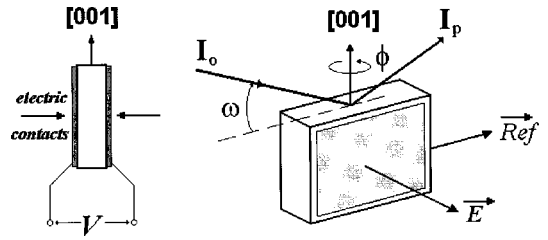

FIG. 2. Setup for applying $\vec{E}$ allowing for both rocking curves (ω) and Renninger scan (ϕ) measurements. $\vec{E}=E_y\hat{y}$.

values obtained from the experiment to make them as easier as possible. Hence we have obtained

$$\frac{\Delta a}{a}=-1.463\times10^{-2}\Delta(\phi^{101}-\phi_0)-5.173\times10^{-2}\Delta(\omega^{006}_{\mathrm{Bragg}})-0.281\Delta(\phi^{200}-\phi_0), \tag{21}$$

$$\frac{\Delta b}{b}=3.673\times10^{-2}\Delta(\phi^{101}-\phi_0)+4.025\Delta(\phi^{020}+\phi_0)+0.281\Delta(\omega^{006}_{\mathrm{Bragg}})-4.471\Delta(\phi^{200}-\phi_0), \tag{22}$$

$$\frac{\Delta c}{c}=-1.723\times10^{-2}\Delta(\phi^{101}-\phi_0)-3.923\times10^{-2}\Delta(\omega^{006}_{\mathrm{Bragg}})+2.097\times10^{-2}\Delta(\phi^{200}-\phi_0), \tag{23}$$

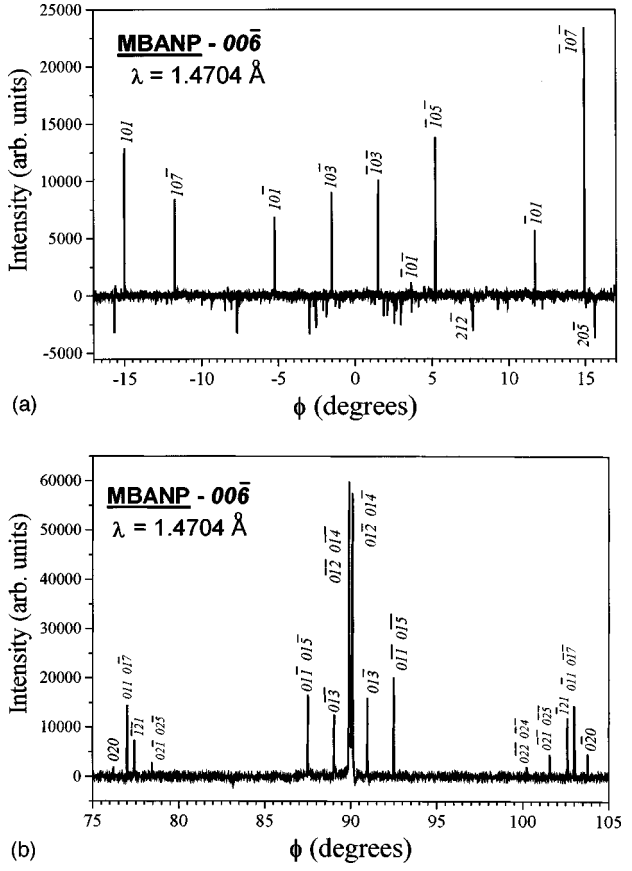

FIG. 3. (a) Portion of the Renninger scan around $\phi=0°$ position. (b) Symmetry mirror which appears around $\phi=90°$ position.

TABLE II. Angular positions of the chose secondary reflections.

hkl	ϕ_{entrance}(deg)	ϕ_{exit}(deg)
200	197.6257	342.5513
020	76.2237	283.7763
101	194.9490	345.0510

and

$$\Delta\beta=-0.214\Delta(\phi^{101}-\phi_0)-0.128\Delta(\omega^{006}_{\mathrm{Bragg}})+0.261\Delta(\phi^{200}-\phi_0). \tag{24}$$

6. Piezoelectric coefficients as a function of the ''effective'' strain

Now, one can use Eqs. (5)–(8) to write down the piezoelectric coefficients as a function of the variation in the diffraction peak positions. By taking $\Delta a/a,\Delta b/b,\Delta c/c$, and $\Delta\beta$ from Eqs. (21)–(24), the coefficients d_{22} and d_{23} are directly determined from

$$E_y d_{22}=\frac{\Delta b}{b}\equiv\varepsilon_{d_{22}} \tag{25}$$

and

$$E_y d_{23}=\frac{\Delta c}{c}\equiv\varepsilon_{d_{23}}, \tag{26}$$

while the remaining two coefficients are obtained from

$$E_y d_{25}=-\Delta\beta+0.080\left(\varepsilon_{d_{23}}-\frac{\Delta a}{a}\right)\equiv\varepsilon_{d_{25}} \tag{27}$$

and

$$E_y d_{21}=1.006\frac{\Delta a}{a}-0.006\varepsilon_{d23}+0.080\varepsilon_{d25}\equiv\varepsilon_{d21}. \tag{28}$$

In other words, the slopes of the curves E_y versus $|\varepsilon_{d_{ij}}|$ allow for the determination of the desired coefficients being $|\varepsilon_{d_{ij}}|$ the deformation produced by the coefficient d_{ij}.

III. EXPERIMENT

The data collection for this study was carried out using the high resolution Renninger scanning equipment on station 16.3 of the Synchrotron Radiation Source, CCLRC Daresbury Laboratory (UK).[26] The station allows measurements with step sizes 0.0002° and 0.0005° in ω and ϕ axes, respectively. Samples were prepared by cleaving slices from high quality single crystals grown by crystallization from solution in methanol at low temperatures.[27,28] In all cases the primary reflection was $(00\bar{6})$. Typical sizes of the samples used in this work were 10 mm×10 mm×1–3 mm (the smallest being the face where x-ray incident beam diffracts).

The electric field was generated by a variable voltage, low current dc power supply and applied to the samples via wires running from the power supply to small bolts attached to the metal tabs of the sample holder. Some conductive sponge (kindly supplied by SGL Carbon Group, Meitingen, Ger-

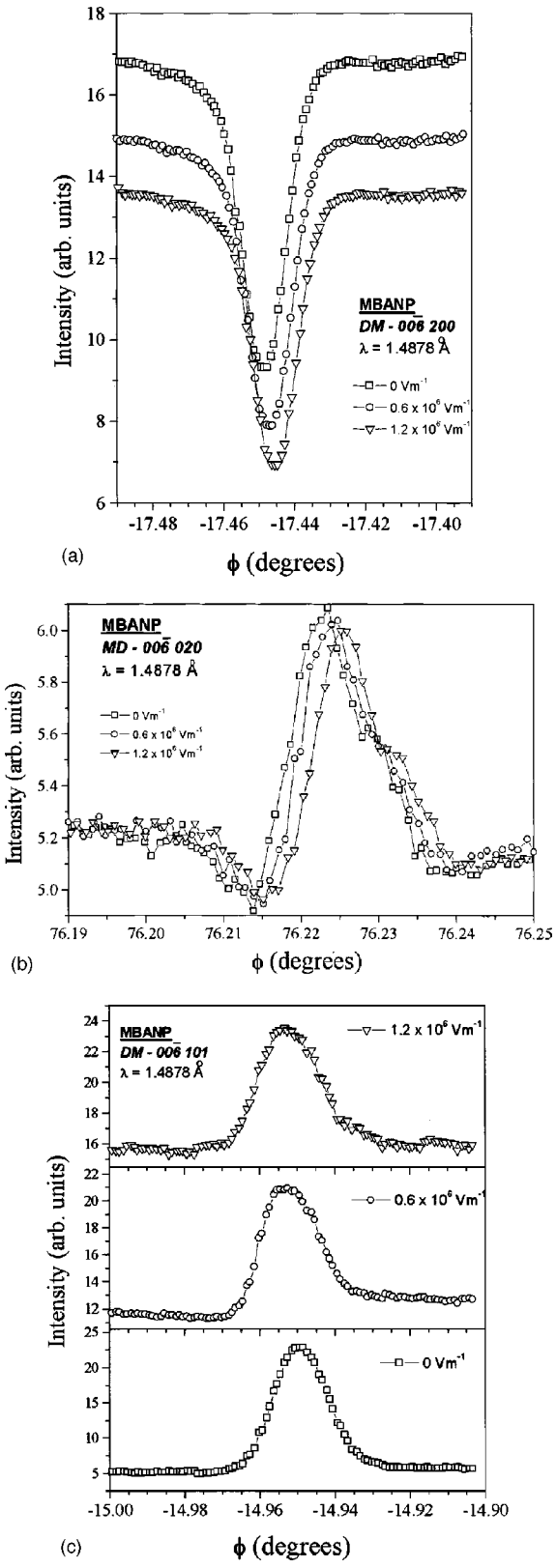

FIG. 4. (a) Multiple diffraction (200) peak as a function of the applied electric field. (b) Multiple diffraction (020) peak as a function of the applied electric field. (c) Multiple diffraction (101) peak as a function of the applied electric field.

many) was positioned between the tabs and sample to improve electrical contact as shown in Fig. 2. The sample holder itself was made of an insulating material so the electric field passed only through the sample. In all experiments $\vec{E}$ was applied parallel to the dipolar $\vec{b}$ axis. The experimental setup was checked by determining the d_{22} piezoelectric coefficient of $LiNbO_3$ and the d_{31}, d_{32}, and d_{33} piezoelectric coefficient of mNA (meta-nitroaniline).[29]

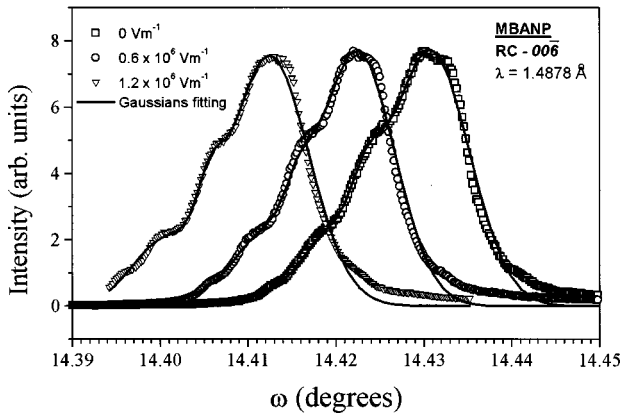

FIG. 5. Rocking curves for $(00\bar{6})$ reflection as a function of the applied electric field.

Figures 3(a) and 3(b) show examples of a Renninger scan taken from an MBANP sample with no applied electric field using radiation of wavelength 1.4704 Å. The symmetry mirror is clearly visible in this scan and corresponds to $\phi = 90°$ [Fig. 3(b)]. Some of the peaks are slightly asymmetric in shape indicative of a crystal of high perfection.

IV. RESULTS AND DISCUSSION

The secondary reflections related to the determination of the piezoelectric coefficients appear in the MBANP Renninger scan at angular positions given in Table II. The primary reflection is $00\bar{6}$ and the $\vec{R}_{ef} = [010]$.

The secondary reflection 200_s at $\phi = 342.5513°$, 020_E at $\phi = 76.2237°$, and 101_s at $\phi = 345.0510°$ were chosen for the measurements. The indices E and S stand for the entrance and exit of the reciprocal node of the Ewald sphere. It should be noticed that when peaks leaving the Ewald sphere are chosen, the negative signal should be used in the equations relating peak position variation and the piezoelectric coefficient.

The electric field was applied in the direction $\vec{E}_y = [010]$ and the field strength: $0\ \mathrm{V\,m^{-1}}$, $0.6\times10^6\ \mathrm{V\,m^{-1}}$, and $1.2\times10^6\ \mathrm{V\,m^{-1}}$. The multiple diffraction peak position variation 200_s for MBANP as a function of the applied E_y is shown in Fig. 4(a). One can directly see that E_y causes just peak shift without any change in its shape. For 020_E, the peak shift as a function of E_y is shown in Fig. 4(b). It is possible to determine the position of each curve despite their forms. Figure 4(c) exhibits the behavior of the multiple diffraction peak 101_s as a function of E_y. Finally, Fig. 5 presents the rocking curve shifts for the $00\bar{6}$ primary reflection. In this figure, it is possible to define several regular peaks due to the mosaicity of the material.[30,31] Then, Table III shows the peak position variations obtained from the above mentioned figures. By using the values in Table III and Eqs. (21)–(24) one can obtain $\Delta a/a, \Delta b/b, \Delta c/c$ and $\Delta\beta$ shown in Table IV.

TABLE III. Renninger scan secondary peak shift as a function of E_y.

hkl	E_y $\times 10^6 (\mathrm{V\,m^{-1}})$	$\Delta(\phi^{hkl} \pm \phi_0)$ $\times 10^{-5}$ (rad)
200	0.6	2.618
	1.2	5.061
020	0.6	0.349
	1.2	0.524
$00\bar{6}$*	0.6	−14.451
(*$\Delta\omega$)	1.2	−31.783
101	0.6	−4.363
	1.2	−8.203

The method based in the rocking curve and in the x-ray multiple diffraction has allowed to probe the variations in the four MBANP crystalline unit cell parameters. It is worthwhile to point out that the values obtained for the angular variation ($\sim 10^{-3}$deg) are of the same order of magnitude of those published in the literature[32] for MNA (2-methyl 4-nitroaniline, monoclinic, point group *m*).

The piezoelectric coefficients can now be determined with Eqs. (25)–(28). Figure 6(a), shows the obtained behavior for $|\varepsilon_{d_{22}}|$ and $|\varepsilon_{d_{23}}|$ with E_y. The curve slopes have provided $|d_{22}| = 24.8(3) \times 10^{-11}\,\mathrm{CN^{-1}}$ and $|d_{23}| = 1.3(1) \times 10^{-11}\,\mathrm{CN^{-1}}$. The remaining coefficients are determined from the slopes of $|\varepsilon_{d_{21}}| \times E_y$ and $|\varepsilon_{d_{25}}| \times E_y$, which appear in Fig. 6(b).

Summing up, we were able to determine four piezoelectric coefficients:

$$d_{21} = 0.2(1) \times 10^{-11}\ \mathrm{CN^{-1}},\ d_{23} = 1.3(1) \times 10^{-11}\ \mathrm{CN^{-1}},$$

$$d_{22} = 24.8(3) \times 10^{-11}\ \mathrm{CN^{-1}},\ d_{25} = 5.9(1) \times 10^{-11}\ \mathrm{CN^{-1}},$$

from the same experimental setup using rocking curves and Renninger scans combined.

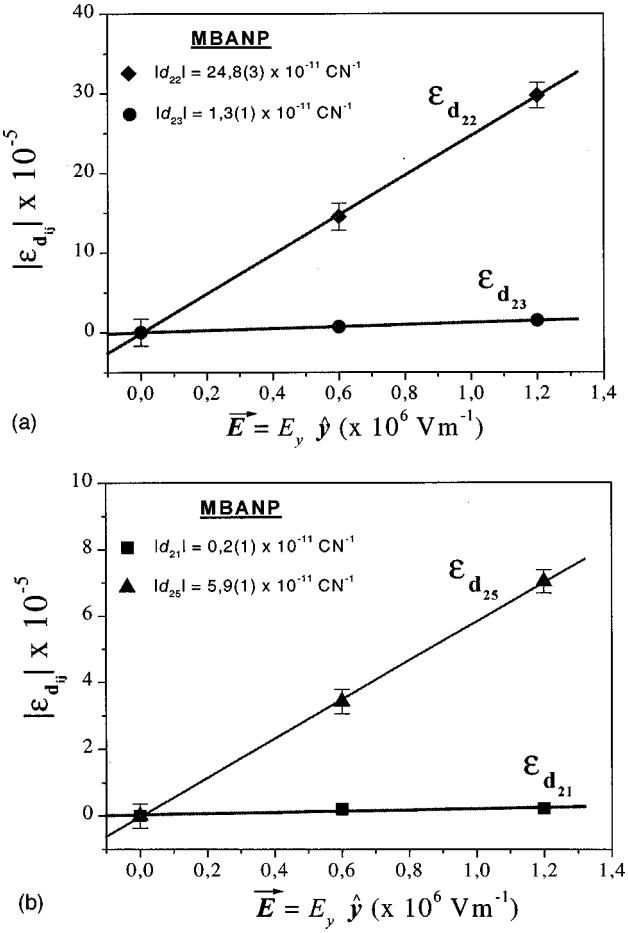

FIG. 6. (a) ''*Effective strain,*'' $\varepsilon_{d_{ij}}$, as a function of the applied electric field. The piezoelectric d_{22} and d_{23} coefficients are determined from the slope of the curves. (b) ''*Effective strain,*'' $\varepsilon_{d_{ij}}$, as a function of the applied electric field. The piezoelectric d_{21} and d_{25} coefficients are determined from the slope of the curves.

V. CONCLUSIONS

In this work, a method was developed to determine piezoelectric coefficients of organic crystals using x-ray multiple diffraction and rocking curves. It uses the measure small changes in the unit cell lattice parameters of a monoclinic crystal due to the application of an external stimulus (electric field). The method was successfully applied to the organic nonlinear optical material MBANP and the four piezoelectric coefficients were determine from one rocking curve and just one Renninger scan, in the same setup as $|d_{21}| = 0.2(1) \times 10^{-11}\,\mathrm{CN^{-1}}$, $|d_{22}| = 24.8(3) \times 10^{-11}\,\mathrm{CN^{-1}}$, $|d_{23}| = 1.3(1) \times 10^{-11}\,\mathrm{CN^{-1}}$, and $|d_{25}| = 5.9(1) \times 10^{-11}\,\mathrm{CN^{-1}}$.

ACKNOWLEDGMENTS

The authors acknowledge the valuable help of the staff of the CCLRC Daresbury Laboratory in the performance of these studies and the staff at the University of Strathclyde for their assistance in preparing the apparatus and samples needed for the experiments. The establishment of facilities for carrying out high resolution XRMD were made possible by funding from the EPSRC (Grant No. GR/E/94739). We also acknowledge the kind support of CNPq and FAPESP (Brazil).

TABLE IV. Deformations in the lattice parameter for MBANP.

$E_y \times 10^6\ \mathrm{V\,m^{-1}}$	$\frac{\Delta a}{a}$	$\frac{\Delta b}{b}$	$\frac{\Delta c}{c}$	$\Delta\beta$ (rad)	$\Delta\beta$ (deg)
0	0	0	0	0	0
0.6	7.571×10^{-7}	-1.452×10^{-4}	6.970×10^{-6}	3.473×10^{-5}	1.99×10^{-3}
1.2	3.420×10^{-6}	-2.975×10^{-4}	1.494×10^{-5}	7.129×10^{-5}	4.08×10^{-3}

*Author to whom correspondence should be addressed. Present address: Instituto de Física, Universidade de São Paulo, CP 66318, 05315-970 São Paulo, SP, Brazil. Electronic address: lhavanci@posseidon.if.usp.br

†Present address: Departamento de Física, Universidade Federal do Ceará, Campus do Pici, CP 6030, CEP 60455-760, Ceará, Brazil.

‡Present address: CCLRC Daresbury Laboratory, Daresbury, Warrington WA 4AD, UK.

[1] *Nonlinear Optical Properties of Organic Molecules and Crystals*, edited by D. S. Chemla and J. Zyss (Academic Press, Orlando, 1987), Vols. 1 and 2.

[2] P. N. Prasad and D. J. Williams, *Nonlinear Optical Effects in Molecules and Polymers* (Wiley-Interscience, New York, 1991).

[3] *Organic Molecules for Nonlinear Optics and Photonics*, Vol. 261 of *NATO Advanced Study Institute, Series B: Physics*, edited by J. Messier, F. Kajazar, and P. Prasad (Kluwer Academic, Dordrecht, 1991), p. 5.

[4] *Principles and Applications of Nonlinear Materials*, edited by R. W. Munn and C. N. Ironside (Blackie and Son, Glasgow, 1992).

[5] R. T. Bailey, F. R. Cruickshank, D. Pugh, and J. N. Sherwood, Acta Crystallogr., Sect. A: Found. Crystallogr. **A47**, 145 (1991).

[6] *Organic Materials for Nonlinear Optics*, edited by R. A. Hahn and D. Bloor, RIC Special Publication **69** (1989); **91** (1991).

[7] R. T. Bailey, F. R. Cruickshank, D. Pugh, and J. N. Sherwood, J. Phys. D **26**, B208 (1993).

[8] D. Pugh and J. O. Morley, *Nonlinear Optical Effects in Molecules and Polymers* (Wiley-Interscience, New York, 1987), Vol. 1, pp. 192–225.

[9] R. T. Bailey, G. H. Bourhill, F. R. Cruickshank, D. Pugh, J. N. Sherwood, G. S. Simpson, and K. B. R. Varma, J. Appl. Phys. **71**, 2012 (1992).

[10] R. T. Bailey, F. R. Cruickshank, P. Pavlides, D. Pugh, and J. N. Sherwood, J. Phys. D **24**, 135 (1991).

[11] R. T. Bailey, F. R. Cruickshank, S. M. Guthrie, B. J. McArdle, H. Morrison, D. Pugh, E. A. Shepherd, J. N. Sherwood, and C. S. Yoon, Mol. Cryst. Liq. Cryst. **166**, 267 (1989).

[12] R. T. Bailey, F. R. Cruickshank, S. M. Guthrie, B. J. McArdle, H. Morrison, D. Pugh, E. A. Shepherd, J. N. Sherwood, C. S. Yoon, R. Kashyap, B. K. Nayar, and K. I. White, J. Mod. Opt. **35**, 511 (1988).

[13] M. Eich, H. Looser, D. Y. Yoon, R. Twieg, G. Bjorklund, and J. C. Baumert, J. Opt. Soc. Am. B **6**, 1590 (1989).

[14] S. L. Chang, *Multiple Diffraction of X-Rays in Crystals*, Springer Series Solid-State Science Vol. 50 (Springer, Berlin, 1984).

[15] R. J. Twieg and C. W. Dirk, IBM Research Report RJ5237 (54077), 1–24 (1986) (unpublished).

[16] J. F. Nye, *Physical Properties of Crystals*, Oxford Science Publications (Clarendon Press, Oxford, 1957) (reprinted in 1995), p. 116.

[17] M. Hart and A. R. Lang, Phys. Rev. Lett. **7**, 120 (1961).

[18] R. Colella, Acta Crystallogr., Sect. A: Cryst. Phys., Diffr., Theor. Gen. Crystallogr. **30**, 413 (1974).

[19] B. Post, Phys. Rev. Lett. **39**, 760 (1977).

[20] S. L. Chang, Phys. Rev. Lett. **48**, 163 (1982).

[21] Qun Shen, Phys. Rev. Lett. **80**, 3268 (1998).

[22] M. Renninger, Z. Phys. **106**, 141 (1937).

[23] S. L. Morelhão, L. H. Avanci, M. A. Hayashi, L. P. Cardoso, and S. P. Collins, Appl. Phys. Lett. **73**, 2194 (1998).

[24] M. A. Hayashi, L. H. Avanci, L. P. Cardoso, J. Bettini, M. M. G. de Carvalho, S. L. Morelhão, and S. P. Collins, J. Synchrotron Radiat. **S6**, 29 (1999).

[25] H. Cole, F. W. Chambers, and H. M. Dunn, Acta Crystallogr. **15**, 138 (1962).

[26] S. P. Collins, R. J. Cernik, B. Fell, C. C. Tang, N. W. Harris, M. C. Miller, and G. Oszlanyi, J. Synchrotron Radiat. **S5**, 1263 (1998).

[27] P. J. Halfpenny, H. Morrison, R. I. Ristic, E. E. A. Shepherd, J. N. Sherwood, G. S. Simpson, and C. S. Yoon, Proc. R. Soc. London, Ser. A **440**, 683 (1993).

[28] P. J. Halfpenny, R. I. Ristic, E. A. Shepherd, and J. N. Sherwood, J. Cryst. Growth **128**, 970 (1993).

[29] L. H. Avanci, L. P. Cardoso, S. E. Girdwood, D. Pugh, J. N. Sherwood, and K. J. Roberts, Phys. Rev. Lett. **81**, 5426 (1998).

[30] S. L. Morelhão, L. H. Avanci, M. A. Hayashi, and L. P. Cardoso, in *Organic Nonlinear Optical Materials and Devices*, edited by B. Kippelen, H. Lackritz, and R. Claus, MRS Symposia Proceedings No. 561 (Materials Research Society, Pittsburgh, 1999), p. 87.

[31] L. H. Avanci, L. P. Cardoso, S. E. Girdwood, J. M. Sasaki, S. L. Morelhão, K. J. Roberts, D. Pugh, and J. N. Sherwood (unpublished).

[32] Antoine Paturle, Heinz Graafsma, H.-S. Sheu, Philip Coppens, and Pierre Becker, Phys. Rev. B **43**, 14 683 (1991).